

4

AERODYNAMIC MODEL DEFINITION

4.1 MODEL SELECTION

The aerodynamic model to be used as the aerodynamic solver within a partitioned FSI model must meet the following requirements: fast computational speed, adaptable to unconventional geometries and low aspect ratios, non-dependant on 3D empirical data.

In the previous section a review was made of the different solvers that can be used to model the aerodynamic forces on a LEI kite. From this, it has been seen that for the degree of accuracy and speed that is being sought, potential flow methods are the best candidate, as they can provide a level of accuracy similar to CFD simulations reducing drastically the computation time.

Within the potential flow methods there are three models that are highlighted for its performance and speed, namely the vortex-lattice method (VLM), the lifting line theory (LLT) and the vortex step method (VSM). With both VLM and LLT, there are studies that have achieved results with a level of accuracy similar to CFD simulations, although with LLT the computational time is much shorter.

The problem with LLT is that for unconventional geometries, such as wings with dihedral and sweep, as well as for low aspect ratio wings, these methods do not give accurate results. According to the studies that have been reviewed, this problem seems to be solved with the VSM, which has a computational time equal to LLT but with more accurate results for such geometries.

That is why VSM has been chosen as the aerodynamic solver for the current FSI model. Nevertheless an LLT will be developed in parallel to compare both models and evaluate the improvement.

4.2 BACKGROUND AND INTRODUCTION

Vortex filament methods are based on Prandtl's classic Lifting Line theory, which since its introduction in the beginning of the 1900s has proven to be able to predict with surprising accuracy the flow past moderate to high aspect ratio unswept wings in incompressible flow. The usefulness of this tool is so great that even today it is widely used in the preliminary calculation of aerodynamic characteristics of finite wings [26].

Prandtl's method uses a single unswept bound vortex to model the circulation around the wing. Due to the Helmholtz theorem, a vortex filament cannot end up in the fluid, so the vorticity system ends up composed of a set of horseshoe vortices, formed by a bound vortex and two trailing vortices, which close at infinity. At any spanwise position, the variation of the strength of the bound vortex Γ is shed as trailing vorticity, which causes induced velocities along the span, and modifies the effective angle of attack seen by the wing. The lifting line is assumed to be unswept, so that the bound vortex at one section does not influence the downwash on other sections, and therefore the downwash is only induced by the trailing vortices, and evaluated at the upstream of the vortex wake. For its implementation, the classical Prandtl's LLT assumes a linear slope for the lift-coefficient of the airfoil sections that compose the wing, typically with a value close to 2π [15].

Nevertheless, the drawbacks of this method were clear, as it results in significant errors for unconventional airfoils and near stall flow conditions, and no profile drag can be estimated. That is why, once the effectiveness of this method for flow prediction on wings with small angles of attack was demonstrated, the focus was on whether it could be modified to take into account the nonlinear nature of the lift slope, especially for angles near stall. Tani [2] is believed to be the first to develop a lifting line method capable of working with nonlinear slopes. His method consists of assuming an initial bound vorticity Γ distribution; in turn, this initial distribution is used to calculate the induced velocities and angles of attack along the span. The angle of attack distribution is then used to look at the corresponding C_l using the lift data for each section. From this distribution of C_l the Γ distribution is recomputed using the Kutta-Juckowski theorem. Then, this iteration is carried out until Γ converges [17].

This method was later explained in detail in the NACA report by Sivells and Neely [6] in 1947, where a tabular procedure for hand-calculation of the method is presented. With this method an analysis of wings up to the onset of stall was performed, i.e. until the angle of attack at which some section of the wing has a C_l equal to the $C_{l_{max}}$ of the airfoil. At higher angles of attack, where the lift slope becomes negative for some sections, this procedure did not converge to correct a correct solution.

In [33], Sears mentions that Von Karman realized that Prandtl's LLT has nonunique solutions for cases where the lift-slope is negative, corresponding to the two angles of attack that have the same C_l . These nonunique solutions can lead to both symmetrical and asymmetrical lift distributions even with a symmetric geometry and flow. This was further investigated by Schairer [5], under the supervision of Sears. Some of these results are presented in [33], which show solutions with asymmetric lift distributions with large associated rolling moments for a small range of angles of attack just after stall [17]. Sears points out that the choice between the symmetric and asymmetrical solution requires the solution of the relative stability of the two flows and concludes that there is a need for further progress on the analysis of wings near and post-stall.

All these were examples of lifting line models where the lifting line is assumed to be straight, so the contribution of the lifting line itself to the downwash is not taken into account. For a more general case in which the lifting line is able to curve, this downwash has to be taken into account, which is not possible using the conventional LLT, as the lifting line has an infinite self-induced velocity. In order to get around this problem a different boundary condition should be defined, in which the angle induced by the system of vorticity is evaluated at a different chordwise location [31].

The first to propose this alternative formulation to the classical LLT was Weissinger [7]. Similarly to the Lifting Line Method, the model presented by Weissinger uses a single chordwise row of horseshoe vortices, with the bound vortex laying at local quarter-chord of each section. The boundary condition of zero normal flow is imposed at the control point, which is located at three-quarter chord. The 3/4 chord location is chosen because the downwash there, in the 2D case, is equal zero-lift line angle of attack, which results in the correct magnitude of the lift force. This method is nowadays commonly referred to as Vortex Step or Weissinger's method.

Pizkin and Levinsky [10] developed a nonlinear Vortex Step method partly based on the iterative method proposed by Tani. The motivation was to create a model able to predict adverse wing stalling characteristics, such as wing drop or loss of roll control. Following on Sears and Von Karman's observations, these characteristics were believed to be caused by the asymmetric lift distribution on fully or partially stalled wings. Unlike in the classical LLT, where the effective angle of attack is calculated as a part of the solution, the change in the control point of the Vortex Step method poses a difficulty in that sense. They overcame this problem by defining the effective downwash angle as $\alpha_{3D} - \alpha_{2D}$, where α_{3D} is the downwash angle at the control point resulting from the entire vortex system and α_{2D} is the induced angle from an infinite bound vortex located at the quarter-chord with strength equal to the horseshoe vortex in question. In this approach, the effects of sweep and dihedral on the effective angle of attack are not included. With this method, different wing planforms and airfoils were studied. The results confirmed that depending on the initial approximation of the vorticity distribution for the iteration, multiple solutions are possible for the lift distribution for post-stall angles of attack. Some of

them are asymmetric even with a symmetric geometry and flight condition. Like in the case of Sears, a need for a method for calculating the relative stability of the different solutions is emphasized.

A few years after Pizkin and Levinsky's study, Anderson, Corda and Van Wie [11] developed a non-linear lifting line method and applied it to wings below and above stall. McCornick [12] presents a similar, independently developed approach where a nonlinear lifting line method is used to study the loss in roll damping for a wing near stall. In both these approaches, no asymmetric lift distributions were shown even with an initial asymmetric distribution, which differs from the observations of Sears and Levinsky.

More recently, Rannenbergh [44] developed a Vortex Step method, based on the principles derived by Pizkin and Levinsky, that takes into account sweep and low aspect ratio, and imposes the tangential flow condition at three-quarter chord. This method was later used by the Makani team, in collaboration with NREL in order to develop KiteFast [49], a tool for calculating the aerodynamic characteristics of rigid kites. According to Damiani, the main author of the report, this method promises accurate solutions for both low and high aspect ratio wings of different shapes, including wings with sweep and dihedral.

4.3 ASSUMPTIONS

The assumptions made regarding the flow properties will be presented below, which are consistent with both the Lifting Line Method and the Vortex Step Method implemented in this project:

- The flow can be divided into two regions the inner and outer region. On one hand, the flow in the inner region represents the airfoil properties, which can be obtained with a variety of methods. On the other hand, the flow outside the region of the airfoil is inviscid, irrotational and incompressible, in order to obtain a potential flow solution.
- The Kutta-Joukowski theorem is fulfilled in each wing section, relating the inner and the outer regions.
- The flow is quasi-steady, meaning that every flow condition can be solved solely in the spatial domain.
- The starting vortex is far downstream and its influence can be neglected.
- **FROZEN WAKE ASSUMPTION**

4.4 VORTEX FILAMENT METHODS

In this section the theorems and considerations common for all models based on the discretization of the wing by means of horseshoe vortices will be explained.

In vortex filaments methods, the vortex particles are arranged into strings, which form a vortex line or filament. These filaments must follow the rules postulated by the Helmholtz and Kelvin theorems [15]:

- Kelvin's theorem : The time rate of change of circulation around a closed curve consisting of the same fluid elements is zero.
- Helmholtz First Theorem : The strength of a vortex filament is constant along its length.

- Helmholtz Second Theorem : A vortex filament cannot start or end in a fluid; it must form a closed path or extend to infinity.
- Helmholtz Third Theorem : The fluid that forms a vortex tube continues to form a vortex tube and the strength of the vortex tube remains constant as the tube moves about.

4.4.1 System of vorticity

In vortex filament methods, it is assumed that the lift force is concentrated in a single bound vortex, called the lifting line. As a consequence, the chordwise load distribution is ignored.

This lifting line is commonly defined as passing through the aerodynamic center of the airfoils of each wing section. This location follows from thin airfoil theory and is convenient since it is the point where the moment coefficient of the airfoil does not vary with angle of attack. The aerodynamic center for an inviscid, incompressible flow at a subsonic speed is located at the quarter chord, and therefore this is the most common location to place the lifting line [47].

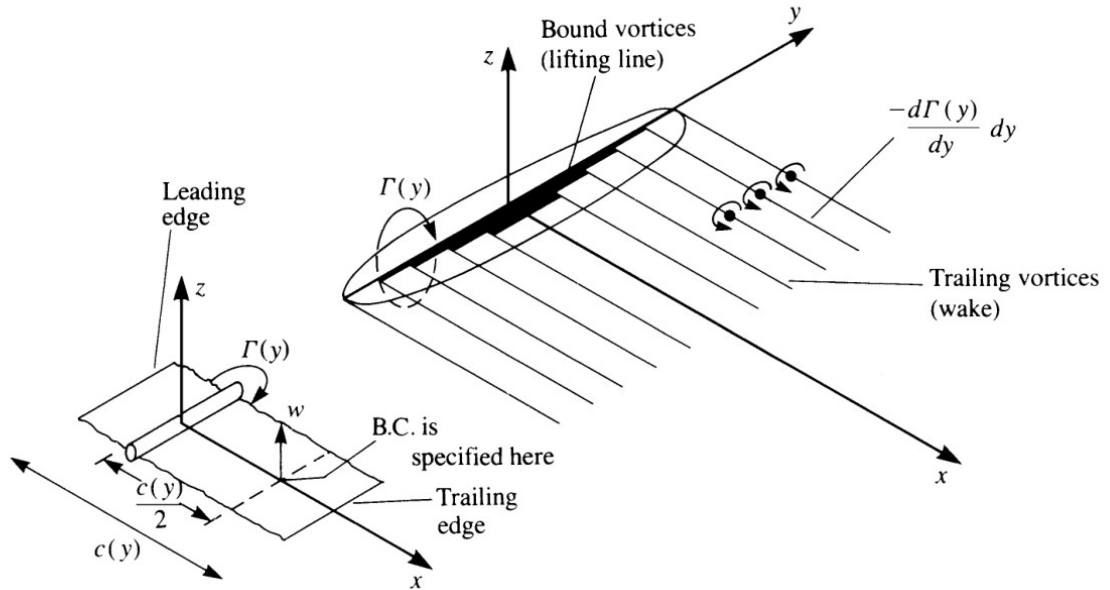


Figure 4.1: Representation of the lifting line model consisting of horseshoe vortices [15]

In addition, this lifting line formed by the bound vortices is assumed to have a variable circulation to take into account the lift variation along the span. As a consequence, there are trailing vortices being shed downstream at each location where a change of circulation is defined.

Two different horseshoe vortex geometries have been tested. The first one is the one proposed by Damiani [49], in the VSM implementation developed by Makani's team. In this, two trailing vortices are shed from the ends of the bound vortex in the direction of the inflow velocity towards infinity. The second one was proposed by Rannenbergh [44], where a VSM is also implemented. In this case, the two trailing vortices follow the airfoil chordwise direction until the trailing edge, and from there they follow the direction of the inflow velocity towards infinity.

These two geometries were tested in the validation phase with different wing geometries. The geometry presented by Rannenbergh resulted in much more accurate results, compared to analytical, CFD and experimental solutions, so it has been decided to implement the latter. In Figure 4.2 it can be seen the schematic of this geometry for a wing panel.

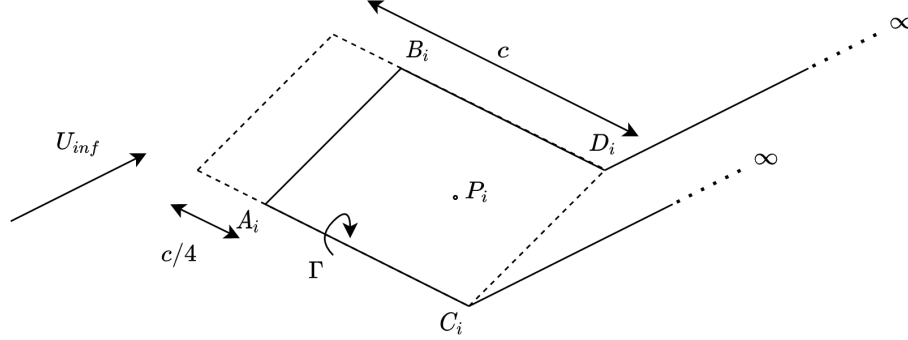


Figure 4.2: Representation of the horseshoe vortex geometry

Given that Helmholtz's second theorem states that a vortex filament can not start or end in space, these trailing vortices are assumed to form a closed loop infinitely downstream. Each of these closed loops is also known as a horseshoe vortex, with which the circulation system is defined (see Figure 4.1).

In Prandtl's classical lifting line theory, the lifting line is assumed to be straight, and the trailing vortices are solely responsible for inducing the downwash which modifies the local angles of attack. On the other hand, on a more general case, where the lifting line is not straight, such as the currently studied VSM, all of the system of vorticity plays a role in the change of the sectional angle of attack [31].

4.4.2 Wake

4.4.3 Computation of induced velocities and core vortex correction

A vortex filament induces a flow field to the surrounding space. The magnitude and direction of this induced flow field can be calculated with the Biot-Savart law. Imagine a curved vortex filament with constant vortex strength Γ , as shown in ???. The velocity induced by a segment $d\mathbf{l}$ to an arbitrary point P is defined by

$$d\mathbf{w} = \frac{\Gamma}{4\pi} \frac{d\mathbf{l} \times \mathbf{r}}{|\mathbf{r}|^3} \quad (4.1)$$

In the development of the LLT and the VSM, the Biot-Savart will be applied to a number of straight vortex paths, with each wing section consisting of 5 vortex filaments, as seen on Figure 4.2.

For a linear path between the points A and B , the induced velocity at the point P is defined by

$$\mathbf{U}_{A,B}(P) = \frac{\Gamma}{4\pi} \frac{\vec{AP} \times \vec{BP}}{|\vec{AP} \times \vec{BP}|^2} \left[\vec{AB} \cdot \left(\frac{\vec{AP}}{|\vec{AP}|} - \frac{\vec{BP}}{|\vec{BP}|} \right) \right] \quad (4.2)$$

where $r_0 = B - A$, $r_1 = P - A$ and $r_2 = P - B$ (as visualized in ???). For the case of the semi infinite trailing legs, the induced velocity can be calculated too by using a limit $r_2 \rightarrow \infty$. For a

straight filament in the direction of the airspeed that goes from point C to infinity, represented by $P_\infty = A + s\vec{v}_a$, where \vec{v}_a is the unitary vector of the airspeed, the induced velocity at the point P can be expressed as:

$$\begin{aligned}
 \mathbf{U}_{A,\infty}(P) &= \lim_{s \rightarrow \infty} \frac{\Gamma}{4\pi} \left(s\vec{v}_a^T \left(\frac{A + s\vec{v}_a - P}{|A + s\vec{v}_a - P|} - \frac{A - P}{|A - P|} \right) \frac{(A - P) \times (s\vec{v}_a)}{|(A - P) \times (s\vec{v}_a)|^2} \right) \\
 &= \lim_{s \rightarrow \infty} \frac{\Gamma}{4\pi} \left(\vec{v}_a^T \left(\frac{A + s\vec{v}_a - P}{|A + s\vec{v}_a - P|} - \frac{A - P}{|A - P|} \right) \frac{(A - P) \times \vec{v}_a}{|(A - P) \times \vec{v}_a|^2} \right) \\
 &= -\frac{\Gamma}{4\pi} \left(1 + \vec{v}_a^T \frac{\vec{AP}}{|\vec{AP}|} \right) \frac{\vec{AP} \times \vec{v}_a}{|\vec{AP} \times \vec{v}_a|^2}
 \end{aligned} \tag{4.3}$$

Lastly, the last interesting case to look at, which will be discussed in the VSM, is an infinite vortex filament. In that case the induced velocities can be expressed as

$$\mathbf{U}_{-\infty,\infty}(P) = \frac{\Gamma}{2\pi} \frac{\vec{AB} \times \vec{MP}}{|\vec{AB} \times \vec{MP}|^2} \vec{AB} \tag{4.4}$$

where M is the position vector of the midpoint from \vec{AB} .

All of the cases just defined have a singularity as the point P approaches the vortex filament, which is clearly seen in [Equation 4.1](#), where the velocity tends to infinity as the radius goes to 0. In order to avoid this discontinuity a vortex core correction is applied. A vortex core radius is given to each vortex filament, assuming a viscous core inside the radius, that is a solid-body like rotation, and a potential vortex outside the core edge. Therefore, if the distance from the point to the filament is smaller than this radius, the induced velocity is made to increase linearly up to the vortex core radius, in the same way as a Rankine vortex. Furthermore, the vortex core radius is calculated differently for the bound and trailing vortices, following the approach of Damiani [\[49\]](#).

Summarizing, the velocities induced by a horseshoe i to a point j can be described as defined in [Equation 4.5](#):

$$\begin{aligned}
\underline{U}_{A_i B_i}(P_j) &= \begin{cases} \frac{\Gamma}{4\pi} \frac{\vec{AP} \times \vec{BP}}{|\vec{AP} \times \vec{BP}|^2} \left[\vec{AB} \cdot \left(\frac{\vec{AP}}{|\vec{AP}|} - \frac{\vec{BP}}{|\vec{BP}|} \right) \right] & \text{if } \frac{|\vec{AP} \times \vec{AB}|}{|\vec{AB}|} > \epsilon_1 \\ \frac{|\vec{AP} \times \vec{AB}|}{|\vec{AB}| \epsilon_1} \underline{U}_{A_i B_i}(P'_j) & \text{otherwise} \end{cases} \\
\underline{U}_{C_i A_i}(P_j) &= \begin{cases} \frac{\Gamma}{4\pi} \frac{\vec{CP} \times \vec{AP}}{|\vec{CP} \times \vec{AP}|^2} \left[\vec{CA} \cdot \left(\frac{\vec{CP}}{|\vec{CP}|} - \frac{\vec{AP}}{|\vec{AP}|} \right) \right] & \text{if } \frac{|\vec{CP} \times \vec{CA}|}{|\vec{CA}|} > \epsilon_2 \\ \frac{|\vec{CP} \times \vec{CA}|}{|\vec{CA}| \epsilon_2} \underline{U}_{C_i A_i}(P'_j) & \text{otherwise} \end{cases} \\
\underline{U}_{B_i D_i}(P_j) &= \begin{cases} \frac{\Gamma}{4\pi} \frac{\vec{BP} \times \vec{DP}}{|\vec{BP} \times \vec{DP}|^2} \left[\vec{BD} \cdot \left(\frac{\vec{BP}}{|\vec{BP}|} - \frac{\vec{DP}}{|\vec{DP}|} \right) \right] & \text{if } \frac{|\vec{BP} \times \vec{BD}|}{|\vec{BD}|} > \epsilon_2 \\ \frac{|\vec{BP} \times \vec{BD}|}{|\vec{BD}| \epsilon_2} \underline{U}_{B_i D_i}(P'_j) & \text{otherwise} \end{cases} \\
\underline{U}_{A_i \infty}(P_j) &= \begin{cases} \frac{\Gamma_i}{4\pi} \frac{1 + \frac{\vec{AP} \cdot \vec{v}_a}{r_1}}{|\vec{AP} \times \vec{v}_a|^2} \vec{AP} \times \vec{v}_a & \text{if } |\vec{AP} \times \vec{v}_a| > \epsilon_2 \\ \frac{|\vec{AP} \times \vec{v}_a|}{\epsilon_2} \underline{U}_{A_i \infty}(P'_j) & \text{otherwise} \end{cases} \\
\underline{U}_{B_i \infty}(P_j) &= \begin{cases} \frac{-\Gamma_i}{4\pi} \frac{1 + \frac{\vec{BP} \cdot \vec{v}_a}{r_1}}{|\vec{BP} \times \vec{v}_a|^2} \vec{BP} \times \vec{v}_a & \text{if } |\vec{BP} \times \vec{v}_a| > \epsilon_2 \\ \frac{-|\vec{BP} \times \vec{v}_a|}{\epsilon_2} \underline{U}_{B_i \infty}(P'_j) & \text{otherwise} \end{cases}
\end{aligned} \tag{4.5}$$

where the points A_i , B_i , C_i , D_i are represented in Figure 4.2, ϵ_1 and ϵ_2 are the core radius of the bound vortex and the trailing vortices, respectively, and P'_j is the radial projection of P_j at the vortex core edge (see Figure 4.3).

The vortex core radius for the bound vorticity is fixed by a cut-off radius parameter δ , as shown in Equation 4.6, which is set to 0.01, following the approach of [18].

$$\epsilon_1 = \delta |\vec{AB}| \tag{4.6}$$

For the trailing vorticity, the vortex core radius is given by Equation 4.7, which models the viscous core growth using the Lamb-Oseen semi-empirical model [16]:

$$\epsilon_2 = \sqrt{4\alpha_0 \nu \frac{|\vec{r}_\perp|}{U_\infty}} \tag{4.7}$$

where α_0 is the Oseen parameter that is 1.25643, ν is the kinematic viscosity of air and \vec{r}_\perp is the position vector from A_i or B_i to the projection of P_j onto the vortex center-line, as shown in Figure 4.3.

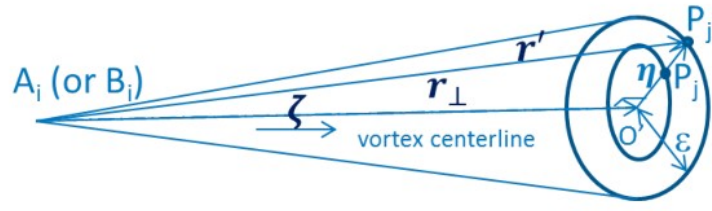


Figure 4.3: Diagram showing the relevant points and vectors for the trailing vortex core correction [49]

4.4.4 Aerodynamic Influence Coefficient (AIC) matrix

Once the horseshoe vortex system and the control points have been defined, the AIC matrix can be computed. The purpose of this matrix is to achieve a way to calculate the relative velocity in each wing section in a fast and efficient way.

The matrix has dimensions of $N \times N$, where N is the number of horseshoe vortices. Each element of the matrix represents the velocity induced by a horseshoe vortex to a certain control point, assuming a unit circulation strength for all vortices. These induced velocities are calculated according to the equations presented in subsection 4.4.3. In this manner, the velocities induced by a random circulation distribution can be solved with the following system of equations, which speeds up the iterative process considerably:

$$\begin{aligned} \mathbf{u} &= \mathbf{AIC}_u \Gamma \\ \mathbf{v} &= \mathbf{AIC}_v \Gamma \\ \mathbf{w} &= \mathbf{AIC}_w \Gamma \end{aligned} \tag{4.8}$$

4.4.5 Circulation distribution calculation

A generic lifting line fundamental equation is used to create a constraint for the distribution of circulation, following the approach implemented in KiteFast [49]. This equation can be derived from the Kutta-Joukowski law (Equation 4.11) as:

$$\rho |\mathbf{U}_\infty \times \Gamma_j| - \frac{1}{2} \rho |\mathbf{U}_{rel} \times \hat{z}_{airf}|^2 c C_l(\alpha_{EFF_j}) = 0 \tag{4.9}$$

where ρ is the air density, \mathbf{U}_∞ is the free-stream air velocity vector, Γ_j is the circulation vector at each section, \hat{z}_{airf} is the local unit vector along the airfoil z-axis, c is the local chord length, $C_l(\alpha_{EFF_j})$ is the 2D lift coefficient as a function of the effective angle of attack α_{EFF_j} .

By solving the system of equations in Equation 4.9, one for each control point in the VSM model, the circulation system can be resolved. The unknowns in Equation 4.9 are Γ , \mathbf{U}_{rel} and α_{EFF} . The latter two, in turn, are a function of the induced velocities and can therefore be expressed as a function of Γ .

With all variables set as a function of Γ , the system of equations is solved by an iterative process, similar to the first one proposed by Tani [2]. It has to be noted that for most cases this method requires of a relaxation factor, which is defined as an input.

4.4.6 Swept flow

In this section an attempt will be made to illustrate the aerodynamic mechanism of sweep and how this effect will be taken into account in the aerodynamic model.

To do so, consider a long wing moving perpendicular to the inflow velocity, as shown in [Figure 4.4](#). The wing is subjected to the velocity w , however, since the wing is moving itself the resultant velocity against the wing is the geometrical sum of u and w . In this scenario, as long as the skin friction is of little importance, the u component does not have a significant influence on the pressure forces produced by the component w . Therefore, the lift could be calculated as:

$$L = \frac{1}{2} \rho A C_L(\alpha) w^2 = \frac{1}{2} \rho A C_L(\alpha) V^2 / \cos(\Lambda)^2 \quad (4.10)$$

Experimental results have also shown that the lift of a yawed wing is proportional to $\cos \Lambda^2$, which confirm that only the component perpendicular to each local wing section effectively affects the pressure forces [8].

In the current implementation, this is taken into account by only taking this component into account when solving the circulation system. In [Equation 4.9](#) this is represented by the modulus of the cross product.

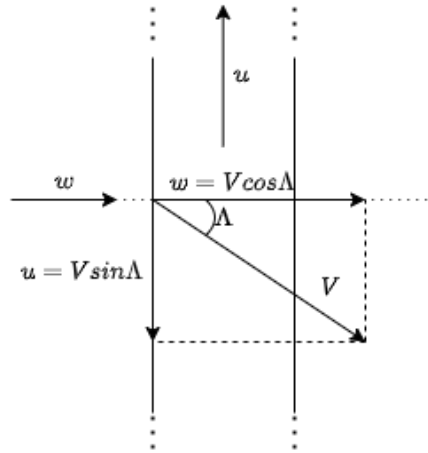


Figure 4.4: Example explaining cross flow principle of swept wings

4.5 SPECIFICS OF 3D NONLINEAR VORTEX STEP METHOD

In this section, a Vortex Step Method based on the principles described by Pizkin and Levinski [10] and Rannenber [44] is presented. In that sense, the system of vorticity is the same as for the LLT. The main difference, as mentioned in the overview, is where the boundary condition is implemented, which for the VSM lies at the local three quarter chord. This assumption stems from Pistolesi's theorem, which states that the angle of attack at the 3/4 chord results in the correct lift associated with the vorticity [44].

Boundary conditions

Once the discretized system of vorticity is set, the possible solutions are given by the linear combinations of each individual Γ_i . The lift associated to each individual section is given by the Kutta-Joukowski law, which states

$$L = \rho U_\infty \times \Gamma \quad (4.11)$$

In order to solve for the values of Γ , a set of boundary conditions must be defined. The classic VSM, as the one defined in [10], uses the no slip condition at the 3/4 chord, meaning that at this point $\mathbf{U}_{rel} \cdot \mathbf{n}_{3/4-c} = 0$, where \mathbf{U}_{rel} is the velocity taking into account the induced velocities created by the system of vorticity, and $\mathbf{n}_{3/4-c}$ is the unitary vector normal to the camber line at 3/4 chord.

The 3/4 chord location of the control point is chosen according to Pistoletti's theorem, which states that at this location, the downwash angle is equal to the angle of the zero-lift line of the section. This theorem is derived from the 2D case, which can be easily verified by picturing a flat plate with an infinite bound vortex at 1/4-chord (see Figure 4.5). According to Thin Airfoil Theory (TAT), the velocity normal to the surface should be zero. At 3/4-chord, the velocities are:

$$V_{n_{3/4}} = V_\infty \sin \alpha - \frac{\Gamma}{2\pi c/2} = 0 \rightarrow \Gamma = \pi c V_\infty \sin \alpha \quad (4.12)$$

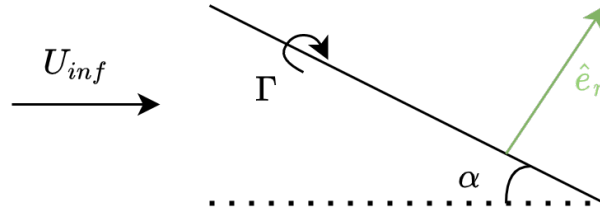


Figure 4.5: Flat plate representation

Then, by applying the Kutta-Joukowski theorem ($l = \rho V_\infty \Gamma$), the C_l slope can be found by combining it with Equation 4.12.

$$C_l = \frac{l}{\frac{1}{2} \rho V_\infty^2 c} = \frac{\rho V_\infty \pi c V_\infty \sin \alpha}{\frac{1}{2} \rho V_\infty^2 c} = 2\pi \sin \alpha \quad (4.13)$$

As it can be seen, the 3/4-chord location yields the correct lift force in the 2D case, a result known as Pistoletti's theorem.

Relative velocity and effective angle of attack

At a control point P_j , the relative velocity and the effective angle of attack can be defined as:

$$\begin{aligned}
\mathbf{U}_{rel}(P_j) &= \mathbf{U}_{\infty}(P_j) + \mathbf{U}_{ind}(P_j) \\
\mathbf{U}_{ind}(P_j) &= \sum_i \mathbf{U}_{ind,i}(P_j) = \sum_i [\mathbf{U}_{A_i B_i}(P_j) + \mathbf{U}_{A_i \infty}(P_j) + \mathbf{U}_{B_i \infty}(P_j) - \delta_{ij} \mathbf{U}_{A_i B_i 2D}] \\
\alpha_{EFF_j} &= \arctan \frac{\mathbf{U}_{rel,j} \cdot \hat{x}_{airf,j}}{\mathbf{U}_{rel,j} \cdot \hat{y}_{airf,j}}
\end{aligned} \tag{4.14}$$

where \mathbf{U}_{ind} is the induced velocity, \hat{x}_{airf} and \hat{y}_{airf} are the unit vectors in the direction of the airfoil's x and y axis and $\mathbf{U}_{A_i B_i 2D}$ is the induced velocity by an infinite vortex filament in the direction of the bound vorticity. The strength of this vortex is equivalent to the strength of the correspondent bound vortex, and it is only applied to the control point within the same horseshoe vortex, as indicated by the Kronecker's delta, which is 0 for all $i \neq j$ and 1 otherwise. This 2D induced velocity term is new compared to the classical LLT, and it is added in order to generalize the formulation for an arbitrary control point location [10].

Correction of the angle of attack

As mentioned above, this way of implementing the boundary conditions results in the correct distribution of circulation, and therefore, in the correct distribution of forces along the wing, assuming that Pistolesi's theorem is valid. Nevertheless, a correct distribution of the magnitude of the forces does not necessarily mean a correct orientation of these.

This concern is raised in Li et. al. [58], where 2D unsteady thin airfoil theory is used to argue the importance of a consistent definition of the direction in which the lift and drag forces are defined. From this study, two important conclusions are drawn relating to generalized lifting line methods, such as the Vortex Step Method;

1. The magnitude of the quasi-steady lift should be determined by the flow at the three-quarter chord location (same as in Pistolesi's theorem).
2. The direction of the quasi-steady aerodynamic forces should be determined by the flow at the quarter chord location.

Following on this approach, once the system of circulation and the aerodynamic have been resolved, the angle of attack is recalculated using the same distribution of circulation but solving the induced velocities at the quarter chord point instead of the three-quarter, which results into the correct direction of the aerodynamic forces according to Li et. al. .

4.6 SPECIFICS OF 3D NONLINEAR LIFTING LINE MODEL

In this section, a Lifting Line Model based on the principles of Prandtl's classical LLT, modified in order to include nonlinear airfoil polars, is presented.

Boundary conditions

In the same way as in the VSM, once the vorticity system is defined, the circulation distribution is solved by applying the Kutta-Joukowski theorem in each wing section. The only difference is that in the classical LLT, the control point is placed at a quarter chord.

Relative velocity and effective angle of attack

At a control point P_j , the relative velocity and the effective angle of attack can be defined as:

$$\begin{aligned}
 \mathbf{U}_{rel}(P_j) &= \mathbf{U}_{\infty}(P_j) + \mathbf{U}_{ind}(P_j) \\
 \mathbf{U}_{ind}(P_j) &= \sum_i \mathbf{U}_{ind,i}(P_j) = \sum_i [\mathbf{U}_{A_i B_i}(P_j) + \mathbf{U}_{A_i \infty}(P_j) + \mathbf{U}_{B_i \infty}(P_j)] \\
 \alpha_{EFF_j} &= \arctan \frac{\mathbf{U}_{rel,j} \cdot \hat{\mathbf{x}}_{airf,j}}{\mathbf{U}_{rel,j} \cdot \hat{\mathbf{y}}_{airf,j}}
 \end{aligned} \tag{4.15}$$

Note that the only difference is that using LLT the term of the 2D induced velocity is not included, as its contribution would be zero, same as the contribution of the bound vortex.

Moreover, since the control point is located at one quarter of the chord, it is not necessary to correct the angle of attack of the aerodynamic forces.

4.7 2D AIRFOIL DATA